Asymmetric MSM sub-bandgap all-silicon photodetector with low dark current

M. Casalino,[1,*] M. Iodice,[1] L. Sirleto,[1] I. Rendina,[1] and G. Coppola[1]

[1]*Istituto per la Microelettronica e Microsistemi (IMM) - Consiglio Nazionale delle Ricerche – Sez. Napoli, Italy*
[*]*maurizio.casalino@na.imm.cnr.it*

Abstract: Design, fabrication, and characterization of an asymmetric metal-semiconductor-metal photodetector, based on internal photoemission effect and integrated into a silicon-on-insulator waveguide, are reported. For this photodetector, a responsivity of 4.5 mA/W has been measured at 1550 nm, making it suitable for power monitoring applications. Because the absorbing metal is deposited strictly around the vertical output facet of the waveguide, a very small contact area of about 3 μm^2 is obtained and a transit-time-limited bandwidth of about 1 GHz is demonstrated. Taking advantage of this small area and electrode asymmetry, a significant reduction in the dark current (2.2 nA at –21 V) is achieved. Interestingly, applying reverse voltage, the photodetector is able to tune its cut-off wavelength, extending its range of application into the MID infrared regime.

OCIS codes: (040.0040) Detectors; (040.5160) Photodetectors; (040.6040) Silicon; (040.3060) Infrared; (250.0250) Optoelectronics; (130.0130) Integrated optics.

References and links

1. M. Casalino, G. Coppola, M. Iodice, I. Rendina, and L. Sirleto, "Near-Infrared Sub-Bandgap All-Silicon Photodetectors:State of the Art and Perspectives," Sensors (Basel) **10**(12), 10571–10600 (2010).
2. M. Casalino, "Near-Infrared All-Silicon Photodetectors," Int. J. Opt. Appl. **2**, 1–16 (2012).
3. B. Aslan and R. Turan, "On the internal photoemission spectrum of PtSi/p-Si infrared detectors," Infrared Phys. Technol. **43**(2), 85–90 (2002).
4. S. Zhu, M. B. Yu, G. Q. Lo, and D. L. Kwong, "Near-infrared waveguide-based nickel silicide Schottky-barrier photodetector for optical communications," Appl. Phys. Lett. **92**(8), 081103 (2008).
5. S. Zhu, G. Q. Lo, and D. L. Kwong, "Low-cost and high-speed SOI waveguide-based silicide Schottky-barrier MSM photodetectors for broadband optical communications," IEEE Photon. Technol. Lett. **20**(16), 1396–1398 (2008).
6. I. Goykhman, B. Desiatov, J. Khurgin, J. Shappir, and U. Levy, "Waveguide based compact silicon Schottky photodetector with enhanced responsivity in the telecom spectral band," Opt. Express **20**(27), 28594–28602 (2012).
7. P. Berini, A. Olivieri, and C. Chen, "Thin Au surface plasmon waveguide Schottky detectors on p-Si," Nanotechnology **23**(44), 444011 (2012).
8. I. Goykhman, B. Desiatov, J. Khurgin, J. Shappir, and U. Levy, "Locally oxidized silicon surface-plasmon Schottky detector for telecom regime," Nano Lett. **11**(6), 2219–2224 (2011).
9. M. W. Knight, H. Sobhani, P. Nordlander, and N. J. Halas, "Photodetection with active optical antennas," Science **332**(6030), 702–704 (2011).
10. A. Akbari, A. Olivieri, and P. Berini, "Subbandgap Asymmetric Surface Plasmon Waveguide Schottky Detectors on Silicon," IEEE J. Sel. Top. Quantum Electron. **19**(3), 4600209 (2013).
11. S. Zhu, H. S. Chu, G. Q. Lo, P. Bai, and D. L. Kwong, "Waveguide-integrated near-infrared detector with self-assembled metal silicide nanoparticles embedded in a silicon p-n junction," Appl. Phys. Lett. **100**(6), 061109 (2012).
12. M. Y. Liu and S. Y. Chou, "Internal emission metal-semiconductor-metal photodetectors on Si and GaAs for 1.3 μm detection," Appl. Phys. Lett. **66**(20), 2673–2675 (1995).
13. S. Averine, O. Bondarenko, and R. Sachot, "High-speed limitations of the metal-semiconductor-metal photodiode structures with submicron gap between the interdigitated contacts," Solid-State Electron. **46**(12), 2045–2051 (2002).
14. J. Shi, K. Gan, Y. Chiu, Y. Chen, and C. Sun, "Metal-semiconductor-metal traveling-wave photodetectors," IEEE Photon. Technol. Lett. **13**(6), 623–625 (2001).
15. W. A. Wohlmuth, M. Arafa, A. Mahajan, P. Fay, and I. Adesida, "InGaAs metal-semiconductor-metal photodetectors with engineered Schottky barrier heights," Appl. Phys. Lett. **69**(23), 3578–3580 (1996).

#193830 - $15.00 USD Received 15 Jul 2013; revised 8 Oct 2013; accepted 9 Oct 2013; published 8 Nov 2013

16. A. K. Okyay, C. O. Chui, and K. C. Saraswat, "Leakage suppression by asymmetric area electrodes in metal-semiconductor-metal photodetectors," Appl. Phys. Lett. **88**(6), 063506 (2006).
17. M. Casalino, L. Sirleto, M. Iodice, N. Saffioti, M. Gioffrè, I. Rendina, and G. Coppola, "Cu/p-Si Schottky barrier-based near infrared photodetector integrated with a silicon-on-insulator waveguide," Appl. Phys. Lett. **96**(24), 241112 (2010).
18. S. M. Sze, D. J. Coleman, Jr., and A. Loya, "Current transport in metal-semiconductor-metal (MSM) structures," Solid-State Electron. **14**(12), 1209–1218 (1971).
19. *Physics of Semiconductor Devices*, S. M. Sze, New York: John Wiley & Sons, (1981).
20. R. H. Fowler, "The analysis of photoelectric sensitivity curves for clean metals at various temperatures," Phys. Rev. **38**(1), 45–56 (1931).
21. *VLSI Technology*, S. M. Sze, New York: McGraw-Hill, (1988).
22. S. Rao, G. Coppola, M. A. Gioffrè, and F. G. Della Corte, "Hydrogenated amorphous silicon multi-SOI waveguide modulator with low voltage-length product," Opt. Laser Technol. **45**, 204–208 (2013).
23. M. Casalino, G. Coppola, M. Gioffrè, M. Iodice, L. Moretti, I. Rendina, and L. Sirleto, "Cavity enhanced internal photoemission effect in silicon photodiode for sub-bandgap detection," J. Lightwave Technol. **28**, 3266–3272 (2010).
24. R. A. Soref, J. Schmidtchen, and K. Petermann, "Large single-mode rib waveguides in GeSi-Si and Si-on-SiO_2," IEEE J. Quantum Electron. **27**(8), 1971–1974 (1991).
25. S. Rao, C. D'Addio, and F. G. Della Corte, "All-optical modulation in a CMOS-compatible amorphous silicon-based device," J. European Opt. Soc. **7**, 12023 (2012).
26. B. Tsaur, M. M. Weeks, R. Trubiano, P. W. Pellegrini, and T. R. Yew, "IrSi Schottky-Barrier Infrared Detectors with 10 pm Cutoff Wavelength," IEEE Electron Device Lett. **9**(12), 650–653 (1988).
27. R. A. Soref, S. J. Emelett, and W. R. Buchwald, "Silicon waveguided components for the long-wave infrared region," J. Opt. A. **8**(10), 840–848 (2006).
28. V. Raghunathan, R. Shori, O. Stafsudd, and B. Jalali, "Nonlinear absorption in silicon and the prospects of mid-infrared silicon Raman lasers," J. Phys. Status Solidi **203**(5), R38–R40 (2006).
29. V. Raghunathan, D. Borlaug, R. R. Rice, and B. Jalali, "Demonstration of a mid-infrared silicon Raman amplifier," Opt. Express **15**(22), 14355–14362 (2007).
30. M. Casalino, G. Coppola, M. Iodice, I. Rendina, and L. Sirleto, "Critically coupled silicon Fabry-Perot photodetectors based on the internal photoemission effect at 1550 nm," Opt. Express **20**(11), 12599–12609 (2012).
31. M. Casalino, L. Sirleto, L. Moretti, F. Della Corte, and I. Rendina, "Design of a silicon resonant cavity enhanced photodetector based on the internal photoemission effect at 1.55 μm," J. Opt. A, Pure Appl. Opt. **8**(10), 909–913 (2006).
32. C. Scales and P. Berini, "Thin-film Schottky barrier Photodetector Models," IEEE J. Quantum Electron. **46**(5), 633–643 (2010).

1. Introduction

Silicon photodiodes are excellent detectors at visible wavelengths, but the development of high-performance photodetectors (PDs) on silicon CMOS platforms at wavelengths of interest for telecommunications has remained an imperative but unaccomplished task so far. However, in recent years, to take advantage of low-cost standard Si-CMOS processing technology, a number of photodetectors have been proposed based on different physical effects, such as: mid-bandgap absorption, surface-state absorption, internal photoemission effect (IPE), and two-photon absorption [1, 2].

The IPE is an attractive approach, because a thin metallic layer, commonly used for local interconnections in the silicon technology, is used as an optical absorber, whose cut-off wavelength is determined by the Schottky-barrier height (SBH) at the metal-Si interface [3]. In recent years, new Si-integrated PDs based on IPE have been investigated both in conventional silicon waveguides and in metallic structures supporting surface plasmon polaritons (SPP). Concerning the former approach, Zhu et al. [4] described a nickel silicide PD based on a Schottky diode integrated into a silicon-on-insulator (SOI) waveguide reporting responsivity and dark current of 4.6 mA/W and 3 nA at −1 V. A similar device from the same group, based on a metal-semiconductor-metal (MSM) configuration shows higher responsivity but, unfortunately, a very high dark current of 100 nA at −1V [5]. Finally, Levy's group fabricated a Schottky PD integrated with a nanoscale silicon bus waveguide achieving a responsivity of 12.5 mA/W at 1550 nm but a dark current of 30 nA at only −0.1 V [6].

Concerning the latter approach, taking advantage of the high confinement of SPPs at a metal/silicon interface, Berini's group investigated the performance of Schottky diode PDs integrated into a metal stripe supporting SPPs at 1550 nm showing a responsivity as high as

#193830 - $15.00 USD Received 15 Jul 2013; revised 8 Oct 2013; accepted 9 Oct 2013; published 8 Nov 2013

0.94 mA/W and a dark current in μA range at an operating reverse bias of 0.1 V in an asymmetric 2-μm-wide 60-μm-long Au strip waveguide [7]. In addition, Goykhman et al. [8] demonstrated a PD based on SPPs propagating along a sub-micron width Au/p-Si interface achieving a responsivity of 0.25 mA/W at 1550 nm and a dark current of 13 nA at an applied 0.1 V reverse bias. Finally, Knight et al. [9] report on the excitation of resonant plasmons in metallic nanoantenna to achieve strong light absorption in a small PD active region. Unfortunately, the responsivity of these nanoantennas depends on the complex optimization of several factors (properties of the involved materials, geometry, efficiency of the uppermost indium tin oxide electrical contact layer) thus a responsivity of only few μA/W at 1550 nm, has been reported as far.

Although IPE has been widely used in Schottky diode structures [4, 6, 10], a few studies have been reported on the IPE in metal-semiconductor-metal photodetectors (MSM-PDs) [11]. Vertically-illuminated MSM-PDs [12, 13] are very attractive compared to the diode counterpart. In fact, by the elimination of heavy doping and thick silicide formation for Ohmic contact, the fabrication process is significantly simplified and it is inherently at lower temperature. In addition, MSM-PDs exhibit larger bandwidth and their speed is limited by the intrinsic RC constant, which can be strongly reduced by making small active area devices. Indeed, MSM-PDs with bandwidth higher than 500 GHz are reported at 780 nm [14]. In contrast, a larger dark current, as compared with the diode counterpart, characterizes the MSM structures because thermionic emission occurs through two Schottky barriers. Nevertheless, the suppression of this dark current can be efficiently achieved using both asymmetric Schottky barriers (through different metals and/or different contact areas [15, 16]) and small contact areas. In waveguide-based MSM-PDs, the absorbing layer, a metal or a silicide, is typically placed on top of the guiding structure [5] and light is absorbed while propagating along the guiding structure. Therefore, achieving a small contact area, without hampering device efficiency, is nontrivial. In addition, in travelling wave photodetectors, device speed can be limited by the velocity-mismatch between electrical and optical signal. It is well known that photodetectors based on IPE suffer from trade-off between responsivity and dark current: the lower the potential barrier, the higher the dark current.

In this paper, we present a SOI waveguide MSM-PD, based on IPE and working at a wavelength of 1550 nm, which is able to tackle this trade off. Taking advantage of the MSM structure, our device is able to increase responsivity lowering the barrier. At the same time, a very low dark current is achieved both by depositing a very small active metal area and by realizing a device with asymmetric electrodes. MSM-PDs allow IPE to take place through a lower potential barrier, because carrier photoemission can occur either through a metal/semiconductor potential barrier (Φ_B) or through the complement of its energy gap (E_g-Φ_B), depending on the applied voltage. The proposed device exhibits a responsivity of 4.5 mA/W, almost two orders of magnitude higher than the diode counterpart [17]. An important novelty of the device is that the absorbing metal is in contact with silicon only on the vertical wall of the optical waveguide, i.e. this absorbing metal is placed strictly around the vertical output facet of the rib waveguide (1.5 μm × 2 μm). This small junction area of only 3 μm^2 enables a bandwidth of 1 GHz to be produced limited only by the time transit of the carriers in the depletion layer. In addition, because of the small junction area and an electrode asymmetry (obtained employing different metals and different contact areas [15, 16]), a very low dark current of 2.2 nA is obtained. Finally, a further increase in responsivity can be achieved reducing the SBH by the applied reverse bias, showing potential for cut-off wavelength tuning.

2. Internal photoemission in MSM structures and photodetector design

In the proposed MSM structure, the electrode asymmetry was achieved by employing as metal contacts copper (Cu) and aluminum (Al), two metals intensively employed in the semiconductor industry for their low resistivity. In Fig. 1(a), a representative band diagram of an Al/p-Si/Cu photodetector is depicted. If a positive voltage is applied to the Al contact (anode) with respect to Cu contact (cathode), the Al/p-Si junction is reverse biased (Al/p-Si)

#193830 - $15.00 USD Received 15 Jul 2013; revised 8 Oct 2013; accepted 9 Oct 2013; published 8 Nov 2013

whereas the Cu/p-Si junction is forward biased. As reported in Fig. 1(a), the sketch of the band diagram defines the SBH at the cathode for electrons and holes (ϕ_N^{Cu} and ϕ_P^{Cu}), the SBH at the anode for electrons and holes (ϕ_N^{Al} and ϕ_P^{Al}), and the SBH lowerings at the cathode ($\Delta\phi_N^{Cu}$) and anode ($\Delta\phi_P^{Al}$) resulting from the image force effect [18].

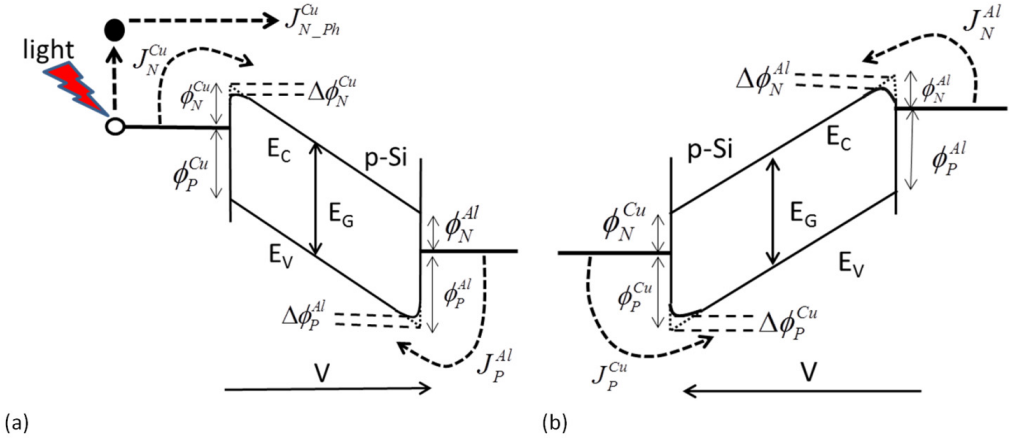

Fig. 1. Corresponding energy band diagram at applied bias greater than V_{FB}: (a) when Al is positively biased with respect to Cu and (b) when Cu is positively biased with respect to Al.

The semiconductor in a MSM-PD is fully depleted when the applied bias exceeds the so-called flat-band voltage V_{FB}, i.e.:

$$V_{FB} = \frac{qN}{2\varepsilon_S} L^2, \tag{1}$$

where q is the electron charge, N the semiconductor doping, ε_S the silicon dielectric constant, and L is the distance between the two electrodes.

Note that for an applied voltage lower than V_{FB}, the variations in the electron and hole SBHs at the anode and cathode are bound by the following relationships:

$$\phi_N^{Cu} + \phi_P^{Cu} = E_g, \tag{2}$$

$$\phi_N^{Al} + \phi_P^{Al} = E_g, \tag{3}$$

where E_g is the Si band-gap (1.12 eV). Thus, the more the applied voltage exceeds the flat-band voltage, the more the potential barrier decreases as a consequence of image forces; also Eqs. (2) and (3) no longer hold. Obviously, similar considerations can be done when a positive voltage is applied to the Cu contact (anode) with respect to Al contact (cathode); in this case, the Al/p-Si and Cu/p-Si junctions will be forward and reverse biased, respectively, and $\Delta\phi_P^{Cu}$ and $\Delta\phi_N^{Al}$ are the respective SBH lowerings at the anode and cathode. A representative band diagram for this case is shown in Fig. 1(b).

We assume that: (a) the dark current is primarily due to thermionic emission, (b) the applied bias is greater than the flat-band voltage, and (c) recombination in the space charge region (SCR), breakdown effects, and surface state transport can be neglected. Hence, the total dark density current for the two different states of polarizations can be written as the sum of the electron injection at the cathode and hole injection at the anode:

$$J_{dark}^{Al\to Cu} = J_N^{Cu} + J_P^{Al} = A_n^* T^2 e^{-\frac{(\phi_N^{Cu} - \Delta\phi_N^{Cu})}{V_T}} + A_p^* T^2 e^{-\frac{(\phi_P^{Al} - \Delta\phi_P^{Al})}{V_T}} \tag{4}$$

#193830 - $15.00 USD Received 15 Jul 2013; revised 8 Oct 2013; accepted 9 Oct 2013; published 8 Nov 2013

$$J_{dark}^{Cu\to Al} = J_N^{Al} + J_P^{Cu} = A_n^* T^2 e^{-\frac{(\phi_N^{Al} - \Delta\phi_N^{Al})}{V_T}} + A_p^* T^2 e^{-\frac{(\phi_P^{Cu} - \Delta\phi_P^{Cu})}{V_T}} \quad (5)$$

where A_n^* and A_p^* are the effective Richardson constants for electrons and holes [18], T the absolute temperature and $\phi_P^{Cu} = 0.74\,eV$ ($\phi_N^{Cu} = 0.38\,eV$) [17], $\phi_P^{Al} = 0.58\,eV$ ($\phi_N^{Al} = 0.54\,eV$) [19] are the potential barriers not yet affected by lowering from image force effects.

For an IPE-based PD, the photo-generated current (I_{Ph}) is linked to the SBH, so the lower the potential barrier, the higher the device efficiency. Thus, for the proposed MSM-PD, the IPE through the lowest potential barrier $\phi_N^{Cu} = 0.38\,eV$ (i.e., biasing Al positively with respect to Cu), as shown in Fig. 1(a), should provide the best responsivity *R,* which is given by the ratio between the photogenerated current (I_{Ph}) and the incident optical power (P_{OPT}) [20]:

$$R = \frac{I_{Ph}}{P_{OPT}} = C \cdot \frac{\left(E_{Ph} - \phi_N^{Cu}(V)\right)^2}{E_{Ph}^2}, \quad (6)$$

where C is the quantum efficiency coefficient, E_{Ph} the photon energy (0.8 eV at 1550 nm), and $\phi_N^{Cu}(V)$ the emitting Schottky barrier depending on the reverse applied voltage due to the image force effect:

$$\phi_N^{Cu}(V) = \phi_N^{Cu} - \Delta\phi_N^{Cu}(V). \quad (7)$$

The lowering of the potential barrier $\Delta\phi_N^{Cu}(V)$ is given by the well-known formula [18]:

$$\Delta\phi_N^{Cu}(V) = \sqrt{\frac{q}{4\pi\varepsilon_S L}(V - V_{FB})}. \quad (8)$$

Unfortunately, a trade-off exists between PD responsivity and dark current: indeed, the lower the potential barrier, the higher the dark current. Taking in account the aforementioned SBH values and Eqs. (4) and (5), the dark density current can be estimated. In particular, we find that the dark density current is mainly due to the thermionic emission of electrons through the lowest potential barrier at the Cu electrode (ϕ_N^{Cu}); also the emission of holes through the higher potential barrier at the Al electrode (ϕ_P^{Al}) is almost four orders of magnitude lower. Therefore, to ensure a low dark current requires fabricating both a very small Cu electrode area and an Al electrode area of no more than four orders of magnitude of the Cu area.

3. MSM photodetector fabrication

The proposed integrated photodetector is illustrated in Fig. 2. As described in the previous section, enhancing the responsivity without increasing the dark current at the same time can be realized by fabricating a very small Cu electrode area (A_{Cu}). This objective was obtained by depositing the absorbing Cu metal strictly around the output vertical facet of a SOI rib waveguide. This active metal is in contact with a large Al pad deposited on the buried oxide layer of the SOI structure, and therefore does not contribute to the dark current or the junction capacitance. A second large Al electrode (A_{Al}), was deposited on the Si substrate to collect the photogenerated current.

#193830 - $15.00 USD Received 15 Jul 2013; revised 8 Oct 2013; accepted 9 Oct 2013; published 8 Nov 2013

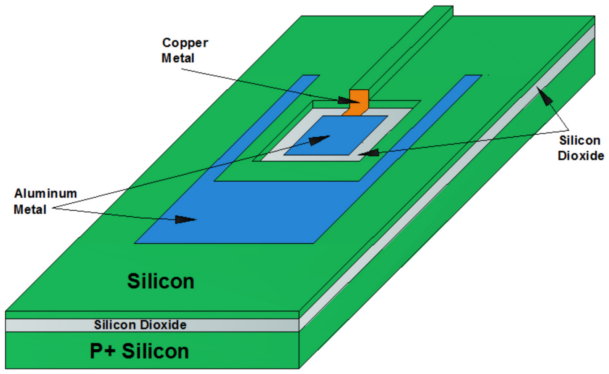

Fig. 2. Schematic of the proposed photodetector integrated with SOI waveguide.

The above-described device was fabricated following a process flowchart fully compatible with microelectronic industry technology [21, 22]. The starting SOI wafer, with a 1.5-µm-thick slightly p-doped (3×10^{12} cm^{-3}) top layer on a 1.0-µm-thick silicon oxide buried layer, was cleaned following a standard RCA procedure [23]. A rib waveguide was defined by a 220-nm-depth reactive-ion etching (RIE) of the top Si layer, with a rib width of 1.5 µm. The rib height was chosen to ensure a single-mode propagation [24, 25]. A second deeper RIE etching was performed to reach the buried oxide and so realize the trench that defines the output vertical waveguide termination.

Next, a Cu metal layer, acting as absorbing element, was deposited. The SOI wafer was covered by photoresist Shipley S1813 and using a photolithographic process, a window around the waveguide termination facet was opened. The sample was dipped in a mixture of hydrofluoric acid (HF) and water (2% of HF) to remove the residual native oxide on the vertical wall of the output waveguide (exposure lasted for only few seconds to prevent removal of the 1-µm-thick buried oxide), rinsed in deionized water, and blown by nitrogen. A 200-nm-thick layer of copper was then thermally evaporated at 3×10^{-6} mbar and 150 °C. During this process the evaporated Cu travels in a straight line between source and substrate (i.e., line-of-sight deposition), depositing also on the vertical wall of the optical waveguide not masked by photoresist. After a photoresist lift-off process, a Cu area of about A_{Cu} = 1.5 µm × 2 µm = 3 μm^2, was obtained. Finally, two 200-nm-thick Al pads were deposited by thermal evaporation at 3×10^{-6} mbar and 150 °C and patterned by a lift-off process of Shipley S1813 photoresist.

In Fig. 3, a top view of the device, acquired by an optical microscope (LEICA DM6000M), is presented. Note that, whereas an Al pad is in direct contact with the top silicon layer, the other (connecting the Cu metal) lies on the oxide layer; for this reason, it does not contribute to either the dark current or the junction capacitance. The Fig. 3 inset shows details of the patterned copper element deposited on the Si/SiO_2 edge and placed at a distance of about L = 45 µm from the Al collection metal.

#193830 - $15.00 USD Received 15 Jul 2013; revised 8 Oct 2013; accepted 9 Oct 2013; published 8 Nov 2013

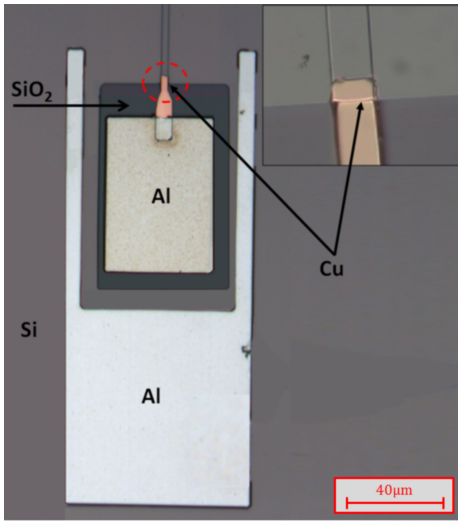

Fig. 3. Top view of the fabricated MSM photodetector acquired by optical microscope; the inset details the patterned copper element deposited on the Si/SiO_2 edge (natural colors).

4. Experimental results

In this section, performances of the proposed asymmetric MSM-PD from the I-V characteristic, responsivity, and bandwidth are reported.

4.1. Current-Voltage characteristic

The device current-voltage (I-V) characteristic are presented in Fig. 4. Note that positive voltage refers to a Cu electrode positively polarized with respect Al and vice-versa for negative reverse voltage. Because of the low Cu/p-Si junction area, a very low reverse current is achieved. In particular, its value is lower than about 2.2 nA for biasing up to −21 V (see inset of Fig. 4). From the I-V characteristic, the potential barriers in the proposed MSM structure can be derived. At a V_{FB} of about 5 V (deduced by the change in slope of the device I-V characteristic in both the forward and reverse regions [18]), the semiconductor is fully depleted and no potential barrier lowering occurs ($\Delta\phi_N^{Cu} = \Delta\phi_P^{Al} = 0$). With values A_{Cu} = 3 μm^2 and A_{Al} = 28419 μm^2 measured by optical microscope, the potential barriers derived using Eqs. (2)-(5) are: $\phi_P^{Al} = 0.53\,eV$, $\phi_N^{Al} = 0.59eV$, $\phi_P^{Cu} = 0.79eV$, and $\phi_N^{Cu} = 0.33eV$. Interestingly, $\phi_P^{Al} = 0.53eV$ and $\phi_P^{Cu} = 0.79eV$ are in very good agreement with those reported in the literature ($\phi_P^{Al} = 0.58\,eV$ [19] and $\phi_P^{Cu} = 0.74eV$ [17]) and used to design the proposed photodetector. Of course, ϕ_N^{Al} and ϕ_N^{Cu} are simply derived by Eqs. (2) and (3).

#193830 - $15.00 USD Received 15 Jul 2013; revised 8 Oct 2013; accepted 9 Oct 2013; published 8 Nov 2013

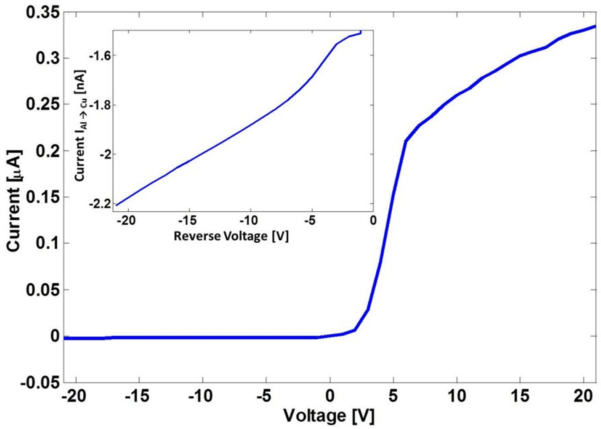

Fig. 4. I-V characteristic of the Cu/p-Si Schottky diode (forward current is obtained biasing Cu positively with respect to Al). The inset gives the rescaled device dark current (biasing Al positively with respect to Cu).

4.2. Responsivity measurements

The photodetector responsivity was estimated by launching into the SOI waveguide an unpolarized near-infrared light beam at 1550 nm and measuring the photogenerated currents while a bias voltage was applied across the device. In particular, a lensed optical fiber, with a spot size of 3 μm, was used to couple the light beam into the rib waveguide. Optical power (ranging from 0.3–0.9 mW) coming out from the lensed optical fiber, was measured using a calibrated power meter (Newport 1931-C). The coupling and waveguide transmission losses were evaluated in a numerical simulation and a value of about 6 dB was estimated [17]. Finally, the photocurrent was measured with a sourcemeter (Keithley 2410) used also to apply the bias voltage.

In Fig. 5, for different applied reverse biases, the linear absorption-induced photogeneration current is given as a function of the optical power estimated to propagate in the silicon waveguide.

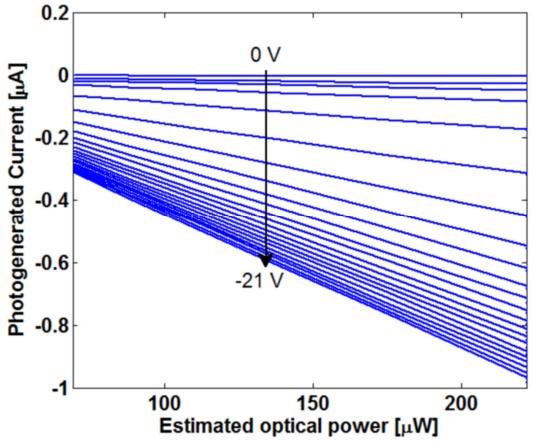

Fig. 5. Photogenerated current at 1550 nm as a function of the estimated optical power under various reverse voltages ranging from 0–21 V in steps of 1 V.

From Fig. 6, we find that the responsivity increases on increasing the reverse applied voltage where it reaches a maximum value of about 4.5 mA/W at –21V.

#193830 - $15.00 USD Received 15 Jul 2013; revised 8 Oct 2013; accepted 9 Oct 2013; published 8 Nov 2013

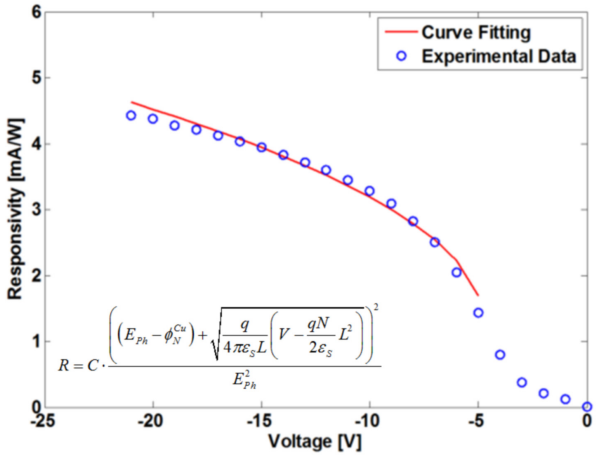

Fig. 6. Responsivity vs reverse voltage applied at 1550 nm. The data has been fitted by a curve using equation reported in the inset.

In addition, from Fig. 6, we observe that there is a change in the slope of curve around V_{FB}, owing to two different mechanisms underpinning photogeneration. Below V_{FB} an increase in reverse bias increases the depletion region width, reducing the recombination in the quasi-neutral region of the photoexcited carriers. Above V_{FB}, the responsivity improvement can be ascribed to SBH lowering. The values of the potential barrier lowering can be estimated fitting the experimental values displayed in Fig. 6 using an equation R = R(V) obtained by combining Eqs. (6)-(8) and (1). The experimental data has been fitted by the relation embedded in Fig. 6. The quantum efficiency coefficient *C* of Eq. (6) was chosen as fitting parameter. After calculating *C*, Eq. (6) is inverted to extract the values of $\phi_N^{Cu}(V)$ that are reported in Fig. 7.

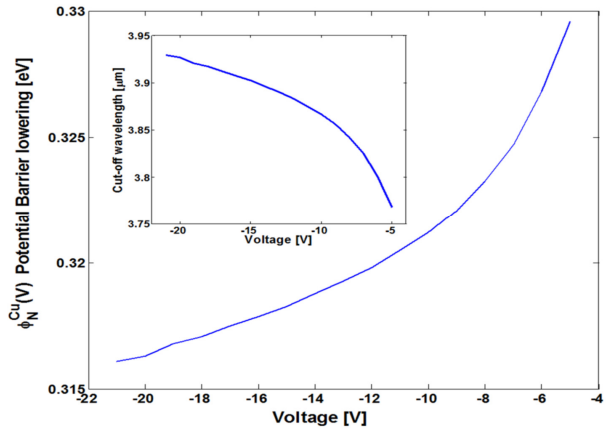

Fig. 7. Cu/Si Schottky barrier vs the applied reverse bias. The inset plots the device cut-off wavelength vs reverse voltage.

It is well-known that depending on the height of the metal semiconductor barrier, the cut-off wavelength of Schottky photodiodes changes according to the following formula [26]:

$$\lambda_{cut-off}(V) = \frac{1.24}{\phi_N^{Cu}(V)}. \tag{9}$$

In the inset of Fig. 7, the tuning of $\lambda_{cut\text{-}off}$ by the reverse applied voltage is given, showing an extension of more than 4%. Tuning of the SBH is generally obtained by engineering the materials (metal or semiconductor) forming the Schottky junction, but unfortunately this is

#193830 - $15.00 USD Received 15 Jul 2013; revised 8 Oct 2013; accepted 9 Oct 2013; published 8 Nov 2013

not a reversible approach. In contrast, the proposed device enables tuning $\lambda_{cut\text{-}off}$ simply by applying a reverse bias. Moreover, as the inset shows, the proposed device has the potential to extend its application into the mid-infrared (MIR) wavelength range. The spectral region beyond 2 μm is of interest for silicon four-wave mixing, because two-photon absorption and the resulting free-carrier absorption are reduced as the combined energy of two photons becomes less than the bandgap energy of silicon [27, 28]. Thus, silicon could potentially be an attractive parametric nonlinear optics platform for applications in which a MIR PD is of vital importance, including free-space communication, chemical and biomolecular sensing, and infrared spectroscopy [29].

4.3. Device bandwidth

The frequency response was measured by launching an externally modulated CW 1550 nm laser beam into our integrated photodiode. A RF signal from a signal generator (Rohde&Schwarz SM300) was applied to the optical modulator (Covega Mach-10 002) to obtain an optical sinusoidal signal with a frequency ranging from 9 KHz to 3 GHz. The electrical output of the photodetector, collected using microwave probes, was measured with a spectrum analyzer (Rohde&Schwarz FS300) using a bias tee. The bias tee was also used to bias the MSM photodetector with a reverse voltage. The whole measurement set-up was tested and calibrated on a commercial InGaAs detector with a 1.2 GHz bandwidth (Thorlabs DET01CFC).

The photodetector frequency response, given by the normalized output of the spectrum analyzer as a function of laser frequency modulation, is reported in Fig. 8. The measured −3dB bandwidth, with a reverse voltage of −21V, is about 1 GHz. The experimental data of Fig. 8 can be fitted by the transfer function of a 2nd-order low-pass filter.

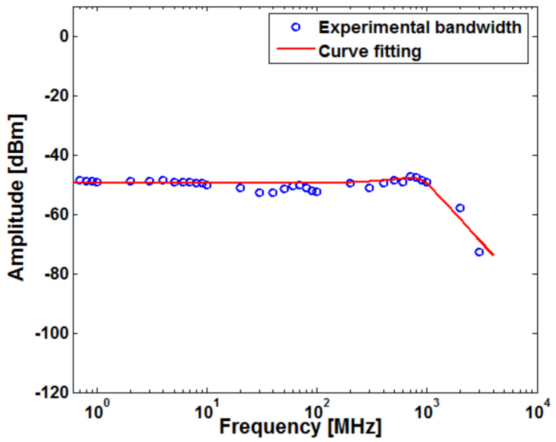

Fig. 8. Experimental device bandwidth and its curve fitting.

At a bias higher than the flatband voltage, the silicon region between the metal contacts can be considered fully depleted and as consequence all photogenerated electrons swept out at a rate bounded by the velocity saturation v_{sat}. In this regime, most carriers leave the photodetector through drift rather than diffusion. Under such conditions, it is well known that the response time of Schottky device is primarily determined by both the RC time constant and carrier transit times. Nevertheless, for a transit-time-limited device, the bandwidth is:

$$f_{3dB} = \frac{2.4}{2\pi\tau_{tr}} = \frac{0.45}{L} v_{sat}. \tag{10}$$

Regarding the proposed device, with the distance between two contacts of L = 45 μm and a silicon saturation velocity of $v_{sat} = 10^7$cm/s [19], a f_{3dB} of about 1 GHz is estimated. This value agrees with that measured and reported in Fig. 8. The first remark on this result is that

#193830 - $15.00 USD Received 15 Jul 2013; revised 8 Oct 2013; accepted 9 Oct 2013; published 8 Nov 2013

the photodetector speed is directly proportional to distance L, thus the bandwidth could be further increased by reducing its value. Alternatively, if the Al contacts are too close to the waveguide an increase in optical absorption could result. Finally, note that, because the photodetector is not a distributed structure, the bandwidth is not limited by the velocity-mismatch between microwave and lightwave.

5. Conclusions

The design, fabrication, and characterization of a low dark current SOI waveguide asymmetric MSM PD based on IPE and working at 1550 nm has been reported. The main novelty of the structure is that the absorbing metal is in contact with silicon only on the vertical wall of the optical waveguide enabling the device to tackle typical responsivity/dark current trade-off afflicting IPE-based devices. By lowering the potential barrier, an increase in responsivity can therefore be obtained without hampering their dark currents. Taking advantage of both a small contact area of about 3 μm^2 and an electrode asymmetry, a significant reduction of dark current of 2.2 nA at −21 V, has been demonstrated. A transit-time-limited bandwidth of 1 GHz has been experimentally measured showing that, because of the negligible junction capacitance, this value could be further increased by scaling down the device size. Moreover, a maximum measured responsivity of 4.5 mA/W makes the device suitable for power monitoring applications. Finally, the device exhibits the capability to extend its wavelength cut-off under an applied reverse bias and could be useful for applications in the mid-infrared regime.

Unfortunately, the device responsivity is greatly afflicted by losses due to reflections of the travelling radiation on the Cu metal layer; hence only a small amount of light can be effectively absorbed (we have estimated that only 9% of the incoming radiation can be absorbed if the Cu layer is so thick that transmitted light can be neglected). This drawback could be overcome by creating an optical microcavity [30, 31] fabricated by etching deep trenches on the silicon rib waveguide. In addition, a further increase in responsivity can be obtained by thinning the metal to increase the probability of carrier emission [32] into the semiconductor. Furthermore, because Cu forms deep-level traps in Si hampering device performance, in future devices it would be beneficial to avoid the direct deposition of Cu on Si by interposing a very thin titanium layer, which blocks diffusion without perturbing the potential barrier.

Acknowledgments

This work was partially supported by the Italian Ministry of University and Research under grants PON PANDION 01_00375.

#193830 - $15.00 USD Received 15 Jul 2013; revised 8 Oct 2013; accepted 9 Oct 2013; published 8 Nov 2013